EARTHQUAKE ENGINEERING AND STRUCTURAL DYNAMICS
Earthquake Engng Struct. Dyn. (2017)
Published online XX in Wiley InterScience (www.interscience.wiley.com). DOI: XX

Seismic Risk Assessment of Liquid Storage Tanks via a Nonlinear Surrogate Model

Konstantinos Bakalis [1,*,†], Dimitrios Vamvatsikos[1] and Michalis Fragiadakis[1]

[1] *School of Civil Engineering, Institute of Steel Structures, National Technical University of Athens, Greece*

SUMMARY

A performance-based earthquake engineering approach is developed for the seismic risk assessment of fixed-roof atmospheric steel liquid storage tanks. The proposed method is based on a surrogate single-mass model that consists of elastic beam-column elements and nonlinear springs. Appropriate component and system-level damage states are defined, following the identification of commonly observed modes of failure that may occur during an earthquake. Incremental Dynamic Analysis and simplified Cloud are offered as potential approaches to derive the distribution of response parameters given the seismic intensity. A parametric investigation that engages the aforementioned analysis methods is conducted on three tanks of varying geometry, considering both anchored and unanchored support conditions. Special attention is paid to the elephant's foot buckling formation, by offering extensive information on its capacity and demand representation within the seismic risk assessment process. Seismic fragility curves are initially extracted for the component-level damage states, in order to compare the effect of each analysis approach on the estimated performance. The subsequent generation of system-level fragility curves reveals the issue of non-sequential damage states, whereby significant damage may abruptly appear without precursory lighter damage states.

KEY WORDS: liquid storage tanks; uncertainty; performance-based earthquake engineering; fragility; demand; capacity;

1. INTRODUCTION

Oil and gas products are generally stored in large-capacity atmospheric tanks. Safeguarding the integrity of such industrial facilities against earthquakes is vital not only for maintaining the flow of essential products and energy resources, but also for preventing any associated socioeconomic consequences of a potential disruption [1]. Ensuring an "appropriate" level of safety tantamount to the importance of liquid storage tanks, mandates the use of state-of-the-art seismic performance assessment techniques that take into account all possible sources of

* Correspondence to: Konstantinos Bakalis, National Technical University of Athens, 9 Iroon Polytechneiou, Athens 15780, Greece.
† E-mail: kbakalis@mail.ntua.gr

uncertainty. Nevertheless, the assessment methodology typically undertaken by engineers is based on design code regulations/provisions and can be summarised in a prescriptive approach that may deliver some acceptable (but actually unknown) level of accuracy, by engaging into a deterministic process where blanket safety factors [2,3] are employed to approximately deliver the required reliability.

In an attempt to rationalise seismic design and assessment procedures, the concept of Performance-based Earthquake Engineering (PBEE) has emerged [4], thus facilitating a logical decision-making process that relies on the probability of exceeding certain capacity thresholds that even make sense to non-engineers [5]. Typically, the procedure begins with the *seismic hazard analysis* [6], where ground motion parameters (e.g. peak ground acceleration, *PGA*) known as seismic intensity measures (*IM*) are characterised in terms of mean annual frequency (MAF) by taking into account all potential earthquake scenarios on the site of interest. It may also be used to identify the scenarios that contribute most to the site-hazard and thus select ground motion records suitable for the *structural response analysis*. Of essence in this case is the estimation of the distribution of certain engineering demand parameters (*EDPs*, e.g. stress, strain, displacement) conditioned on the seismic intensity. Different analysis methodologies can be carried out to derive it, and the choice generally relies on a trade-off between accuracy and computational burden. Normally, one can employ Incremental Dynamic Analysis (IDA) [7] for a wide range of ground motion records and seismic intensity levels, to obtain a refined representation of the *EDP*-*IM* space, bearing in mind that this analysis approach does not allow rigorous record selection to cover up any *IM*-related deficiencies in terms of sufficiency [8]. Closely related is the stripe analysis [9] where different records may be employed at each *IM* level to improve upon an insufficient *IM* [10]. Cloud analysis may similarly be employed using even unscaled records, but requiring some global or local regression in post-processing, plus perhaps some logistic regression to take care of collapse (i.e. global instability) points where non-convergence appears [9]. The subsequent *damage analysis* conveniently summarises the *EDP* distributions into fragility functions [11], thus assigning probabilities of exceedance on certain damage state (*DS*) or limit state (*LS*) capacity thresholds. The aforementioned quantities are finally translated into decision variables through the *loss analysis* that relies on cost data for repair, downtime and casualties, with respect to the damage states examined [12]. The final output is normally in the form of the MAF exceeding a (usually monetary) threshold of interest that engages facility owners and stakeholders into comprehensive mitigation actions.

As much as PBEE has reached a mature state for plenty of mainstream civil engineering structures (e.g. buildings, bridges), there are hardly any provisions regarding its application to industrial equipment structures [13]. Parameters such as the geometry, the toxicity/flammability of the stored materials, and the intrinsic failure modes, make the problem substantially different from buildings or bridges, as the post-earthquake impact may span from operational costs only, to uncontrollable environmental consequences that are often triggered due to the potential leakage of the stored materials [13–15]. The devastating outcome of earthquake events such as Kocaeli (1999) and Tohoku (2011), further enhances the view that comparatively little attention has been paid to liquid storage tanks, even from an academic perspective. Previous research efforts may be summarised to a fragility-based methodology using either costly finite element models [16,17], or available observational (i.e., historical or empirical) data as shown by O'Rourke and So [18]. Empirical fragility curves are also provided by Salzano et al. [19] using the probit function to fit the available data, while Berahman and Behnamfar [20] adopt a Bayesian approach to predict the associated probability of exceedance. Analytical fragility curves for oil storage tanks are available by Iervolino et al. [21], yet they only cover a single failure mode despite the consideration of various geometric characteristics that affect the

DOI: XX

dynamic response of the tank. Other studies [22,23] compare large sets of analytical results to observational ones, while there is at least one attempt to extend this train of thought to the entire plant level [24], where fragility curves from various industrial structures (e.g. atmospheric tanks, pressure vessels) should appropriately be combined to estimate the associated risk.

In any case, from a performance-based point of view, there are several pieces in the existing literature (e.g. structural modelling, damage classification, cost assessment) that are either missing or not adequately substantiated to properly translate the analysis output into decision-making variables for liquid storage tanks. Bearing in mind that the individual steps of the PBEE process are all equally important, this work emphasises the structural response and damage (or fragility) analysis that are of particular interest to structural engineers. In specific, it offers an approach that respects proper uncertainty propagation from all pertinent sources and is based on a three-dimensional (3D) surrogate model, appropriate for efficiently running multiple nonlinear response-history analyses, while also allowing to distinguish parts of the tank to offer different levels of damage resolution: Either localised to individual segments and components or generalised to refer to the entire structure, as needed.

2. MODELLING OF LIQUID STORAGE TANKS

Adopting the PBEE concept for the case of liquid storage tanks requires a series of tasks to be tackled before the MAF of exceeding a specified *LS* capacity is estimated. Of particular concern is the modelling of such complex structural systems. The fluid-structure-interaction, for instance, imposes several constraints related to the computational effort required, and despite the evolution of computer technology, explicitly modelling the contained fluid and the associated contact properties with the tank shell results in costly finite element models. Given that the number of scenarios considered within a performance-based framework is often significantly larger compared to that of code-based methodologies (e.g. 3 or 7 nonlinear response history analyses according to Eurocode 8 [25], vis-à-vis 40-60 analyses for performance assessment [7,9]), simpler surrogate models are required for PBEE applications.

Previous research [26] has shown that earthquake ground motions cause part of the contained fluid to move rigidly with the tank walls (impulsive component), while its remaining portion (convective component) develops a sloshing motion on the free fluid surface (Figure 1(a)). Such observations have led to the development of two-degree-of-freedom (2DOF) approximate models that are suitable for estimating the internal forces and moments, both for anchored and unanchored liquid storage tanks (e.g. [27,28]). Furthermore, the periods of vibration of the two components (i.e. impulsive and convective) are well-separated for practically any tank, thus allowing the decoupling of their respective responses.

Along these lines, Bakalis et al. [29] proposed a 3D single mass surrogate modelling approach for the seismic performance assessment of fixed roof liquid storage tanks. The so-called "Joystick" model is presented in Figure 1(b) along with its fundamental modelling details. It consists of a mass (m_i) that represents the impulsive fluid component, attached to an elastic beam-column element, whose properties are estimated such that the fundamental period of the model is fully aligned to the theoretical solution for the impulsive period [26,27]. The elastic element is connected to *n* rigid beam-spokes that rest on multilinear elastic edge-springs. Those springs are assigned uplift (w) as well as compression resistance properties of a beam (strip) model that extends diametrically on the base plate of the tank, has an effective width $b_w=2\pi R_t/n$ (where R_t is the tank radius), utilises rotational ($k_{\theta\theta}$) and axial (k_{uu}) springs to model the plate-wall interaction, a concentrated force (N_r) and moment (M_r) to take into account the effect of hydrostatic loads, and is supported by an elastic tensionless Winkler soil/foundation

DOI: XX

[29,30] (Figure 1(c)). Essentially, the "Joystick" model is a two-stage model that requires the execution of the base-plate strip model "pre-analysis" step (Figure 1(c)) to determine the properties of the "Joystick" model edge-springs (e.g. vertical force (V) versus uplift, separation length (L), etc.). While the "pre-analysis" step requires a few minutes to complete, the "Joystick" model has the ability to perform response history analysis using multiple ground motion components in seconds, without repeating the relatively time-consuming "pre-analysis" step when a different ground motion record or scale factor is adopted. It is also able to take the effect of the anchor bolts into account, simply by modifying the aforementioned edge-springs through a damageable gap-material, the stiffness of which corresponds to the equally-spaced anchor bolts found on the effective width of each beam-spoke (b_w). Sliding may also be similarly incorporated using suitable friction elements. Overall, the simplified nature of the "Joystick" model offers the ability to model practically any cylindrical liquid storage configuration, regardless of geometry, support conditions and material/fluid properties.

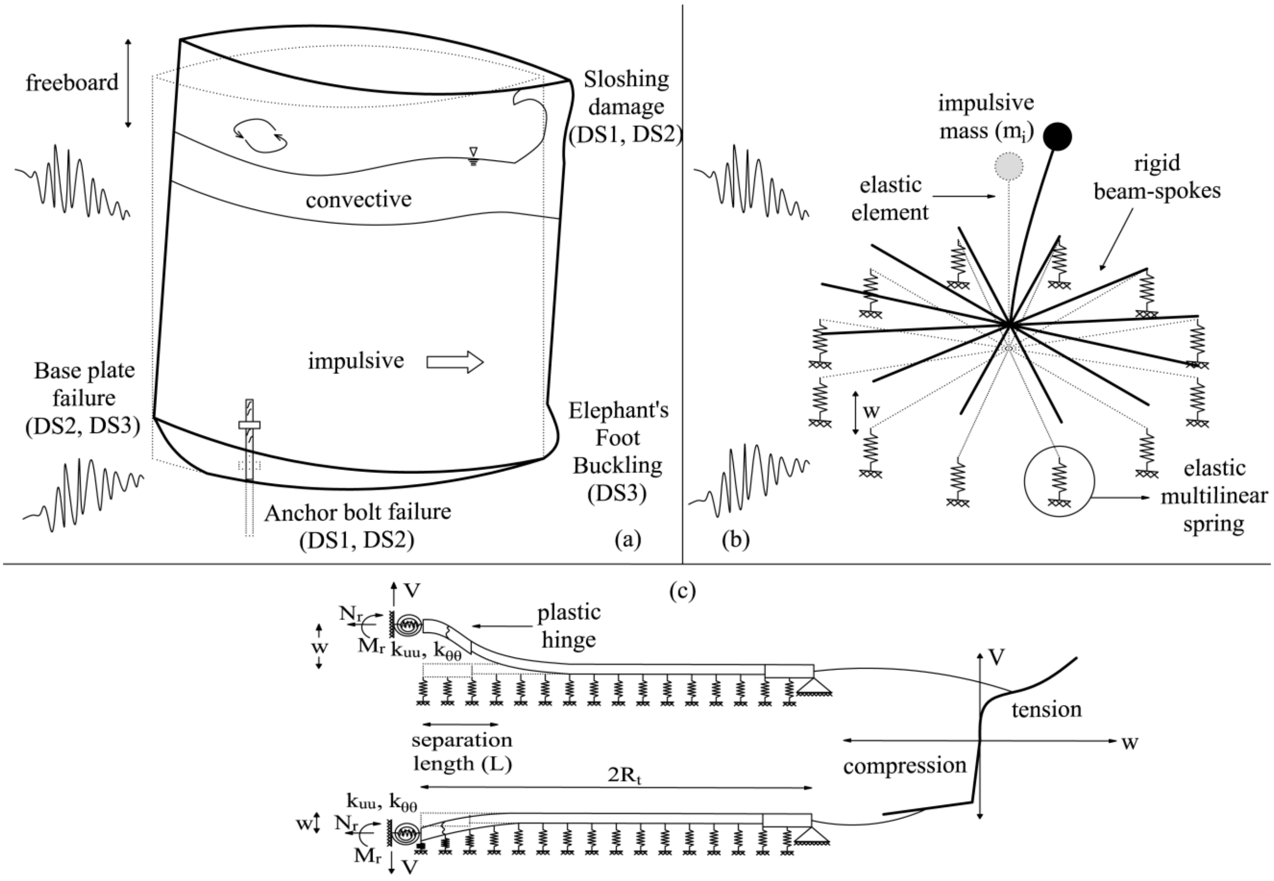

Figure 1: (a) Impulsive versus convective fluid component, failure modes and system-level damage state classification on a fixed roof liquid storage tank. Depending on the presence of anchors, the system is either anchored or unanchored. (b) The "Joystick" surrogate model [29] and its deflected shape. (c) The strip model under tensile and compressive loading.

3. FAILURE MODES

An important consideration for the PBEE application is the ability of simplified models to capture all major modes of failure that may be developed locally on the structural system.

DOI: XX

Regardless of support conditions (i.e. anchored or unanchored), commonly observed modes of failure on liquid storage tanks involve fracture of the base plate due to extreme base plate plastic rotations (θ_{pl}), buckling of the tank shell and sliding. These modes of failure derive from the liquid storage system's trend during ground motion shaking to overturning. As seismic waves arrive on site, the impulsive fluid component imposes pressure on the tank walls, causing excessive overturning moments on the system that may in turn lead to sliding and/or partial uplift of the base plate. The latter results in large-strain deformations on the plate-wall junction that may rupture the base plate. At the same time, the compressive side of the tank suffers from a biaxial stress condition, generated by the compressive meridional and tensile hoop components, which may lead to an elastic-plastic buckling failure. The latter exhibits a characteristic bulge along a considerable part on the tank's circumference, also known as the Elephant's Foot Buckling (EFB). For the case of anchored tanks, damage on the anchor bolts constitutes another potential failure mode. Fracturing of the anchors is also affected by the impulsive-component-induced overturning, as the tension developed on the bolts may often exceed their prescribed ultimate strength and ductility. Note that although anchored liquid storage systems are usually considered fully fixed to the ground, their actual performance can incorporate some rocking/uplift, especially when the anchor bolts begin to yield or fracture. At this point, part of the base plate is uplifted and the response gradually resembles that of the corresponding unanchored case [29]. The convective fluid component on the other hand, determines any kind of damage related to the upper courses of the tank walls and the roof. It is also known to offer additional overturning moments at the base of the system, but its contribution with respect to the impulsive component is marginal for the majority of non-slender tanks, and as a result it is often ignored. The failure modes outlined above are depicted in Figure 1(a).

4. ENGINEERING DEMAND PARAMETERS

Capturing the potential failure modes using surrogate models requires a series of failure criteria to be considered, which are expressed as a function of the engineering demand parameters (*EDPs*) available from the model output. Such criteria are discussed herein for all the aforementioned modes of failure with the exception of sliding, as it requires some elaborate knowledge of the nozzle geometry and mechanical properties. The general view regarding the criteria adopted for the seismic risk assessment of a structure, is that they should remain objective (i.e. neither conservative nor unconservative). In the following, although certain code equations are employed, it should be noted that most of them were presented prior to publication of the codes considered and were not necessarily intended for code-based design. Apparently, the methodology could easily be modified upon the availability of more refined criteria.

4.1. Base plate and wall-to-base connection

The deflected shape of the "Joystick" model (Figure 1(b)), reveals its ability to simulate the uplift mechanism of liquid storage systems, which provides an indirect mapping to local *EDPs* through the base plate strip model (Figure 1(c)). For instance, the base plate plastic rotation can be estimated using either direct measurements from the simplified uplift response analysis of the base plate strip [29,30], or with the aid of the Eurocode 8-4 [2] equation

$$\theta_{pl} = \frac{2w}{L} - \frac{w}{2R_t}, \tag{1}$$

DOI: XX

where w is the base uplift and L is the uplifted part of the tank. Note that Eurocode 8-4 provisions suggest a maximum permissible θ_{pl} value of 0.2rad, while experimental studies suggest that this value is overly conservative, proposing a fracture capacity of 0.4rad instead [31]. Actually, these values are proposed under the condition that fracture occurs outside the weld that connects the plate to the tank wall; therefore, if a weak weld is suspected to be present, the rotational θ_{pl} capacity may need to be reduced.

4.2. *Anchorage*

Anchorage failure is governed by yielding or fracture of the respective anchor bolts. There are many ways to express this kind of failure (e.g. stress, strain, displacement), and most times the choice of the appropriate *EDP* relies on the structural model that has been chosen to predict the response. When the “Joystick” model [29] is adopted, response of the anchor bolts may be estimated through the base uplift that essentially determines their deformation/elongation (δ). Failure may then be captured by assuming that the entire number of anchor bolts corresponding to each spoke (i.e. those along an arc length equal to b_w) are uniformly stressed and respond elastoplastically with a yield-displacement strength (δ_y) and fracture-displacement capacity (δ_u) consistent with the connection ductility.

4.3. *Sloshing*

Sloshing damage is triggered upon the exceedance of the available freeboard d_f, (Figure 1(a)), i.e. the available clearance of the free fluid surface (at rest) to the roof. The response is purely dominated by the maximum convective wave height (d) developed during the earthquake. Given the elastic treatment of this problem, Eurocode 8-4 offers the following simplified equation for the sloshing response prediction

$$d = 0.84 R_t S_a\left(T_c, \kappa_f\right)/g\,, \tag{2}$$

where g is the gravity acceleration and $S_a(T_c, \kappa_f)$ the convective period elastic response spectrum acceleration for an appropriately defined fluid damping (e.g. κ_f=0.5% for water [2], bearing in mind that more sophisticated solutions exist [32]). API-650 [3] also adopts a similar equation using an acceleration coefficient for sloshing wave height calculation in place of the $0.84S_a(T_c,\kappa_f)$ term.

4.4. *Elephant’s Foot Buckling*

Elephant’s Foot Buckling depends on the compressive meridional stress demand (σ_m) developed on the tank shell. This mode of failure is slightly more complex to determine, as the edge-spring force (N) recorded from the “Joystick” model must be converted to stress before it is compared to a critical buckling limit (σ_{EFB}). The latter may be estimated, for instance, according to Rotter’s [33] formula (also adopted by Eurocode 8-4 [2]) as

$$\sigma_{EFB} = \sigma_{c1}\left[1-\left(\frac{pR_t}{t_w f_y}\right)\right]\left(1-\frac{1}{1.12+r^{1.15}}\right)\left[\frac{r+f_y/250}{r+1}\right] \tag{3}$$

$$\sigma_{c1} = 0.6E\frac{t_w}{R_t} \tag{4}$$

DOI: XX

$$r = \frac{R_t / t_w}{400} \tag{5}$$

E is the steel elastic Young's modulus, f_y the corresponding yield strength, t_w the wall thickness, σ_{c1} the ideal critical buckling stress for cylinders loaded in axial compression and p the maximum interior pressure acting on the tank wall. The interior pressure is the direct sum of the hydrostatic (p_h) and impulsive component (p_i). The latter may be estimated by adopting a cylindrical coordinate system, using the non-dimensional coordinates ξ (radial), ζ (height), φ (angle), as:

$$p_i(\xi,\zeta,\varphi,t) = C_i(\xi,\zeta)\rho_f h_f \cos\varphi A(t) \tag{6}$$

C_i is a function that provides the distribution of p_i along the tank elevation, ρ_f is the fluid density, h_f the contained fluid height and $A(t)$ is the impulsive mass absolute acceleration response history [34]. As a side note, the EFB check should not be limited to the lower course of the tank shell where the maximum interior pressure occurs, but should rather be extended to the entire tank elevation, especially when the wall thickness is not uniform. Although one could derive a simple relationship for the stress distribution over height, this step may be ignored as in most cases the lowest course is the most critical one.

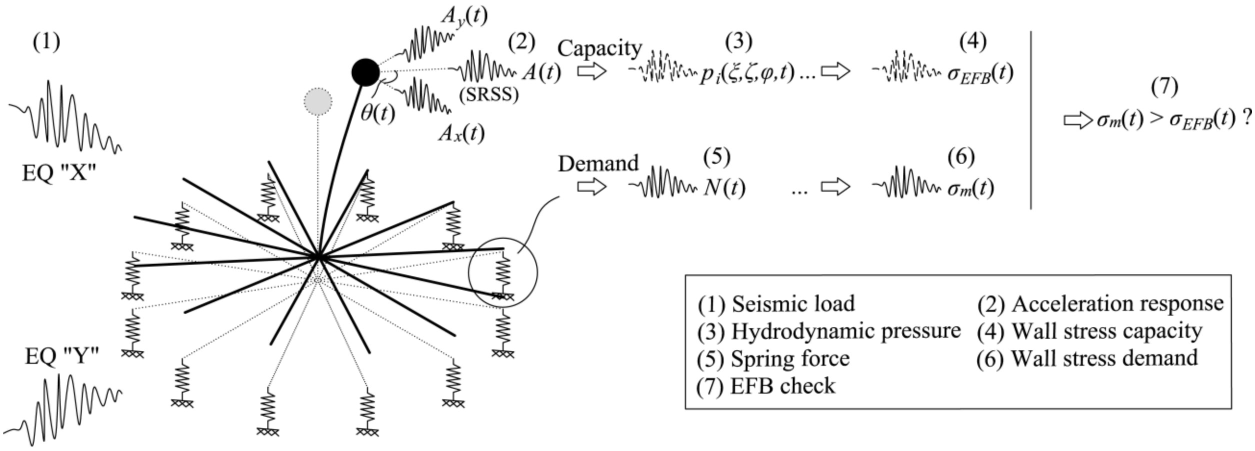

Figure 2: EFB violation check using the "Joystick" model instantaneous demand and deterministic capacity estimates.

4.5. Special considerations for EFB

4.5.1 EFB conditioned on the ground motion record

Eq. (3) provides a useful approximation to assess the occurrence of EFB. Still, its accurate application is not as simple since the stress limit (σ_{EFB}) provided is a decreasing function of the impulsive pressure (Eq. (6)) at each location (φ), and thus the absolute acceleration demand (and hence the seismic intensity). According to Eq. (3)- (6), EFB stress capacity is both location and time-dependent, and so is the corresponding stress demand. Thus, at every time step, $\sigma_m(t)$ and $\sigma_{EFB}(t)$ need to be evaluated for each edge-spring on the "Joystick" model, effectively discretising the continuous tank wall (as well as the associated checks) into n positions. It should be noted that the EFB demand appears to be more sensitive to the base plate discretisation, thus requiring a number of 30-60 spokes, as opposed to other global response parameters (e.g. uplift) where only 8 spokes [29,35] are sufficient. In general, as the tank radius grows, the number of spokes should be increased to achieve a better discretisation, and a good rule of thumb would

DOI: XX

be to target at least an arc length of 2-3m for each spoke.

For a given fraction of time, each evaluation consists of estimating the vector-sum of the longitudinal and transverse component response accelerations (i.e. $A_x(t)$, $A_y(t)$) and its orientation (i.e. $\theta(t)$), vis-à-vis the earthquake (EQ) "X" and "Y" axes (Figure 2). Using Eq. (6), this results in the instantaneous pressure for each spoke located at an angle φ from the vector of $A(t)$. The sum of p_i and p_h determine the instantaneous $\sigma_{EFB}(t)$ capacity of any single spoke. Conversely, the strip model (Figure 1(c)) demand of compressive axial force $N(t)$ at each edge-spring, divided by the corresponding tank wall cross-section, provides the local stress demand $\sigma_m(t)$. Assuming no further uncertainties enter into the estimation of $\sigma_{EFB}(t)$, a straightforward comparison among $\sigma_m(t)$ and $\sigma_{EFB}(t)$ determines violation as shown in Figure 3 for the case of a squat tank, the properties of which are summarised in Table 1 among other configurations that will later be examined.

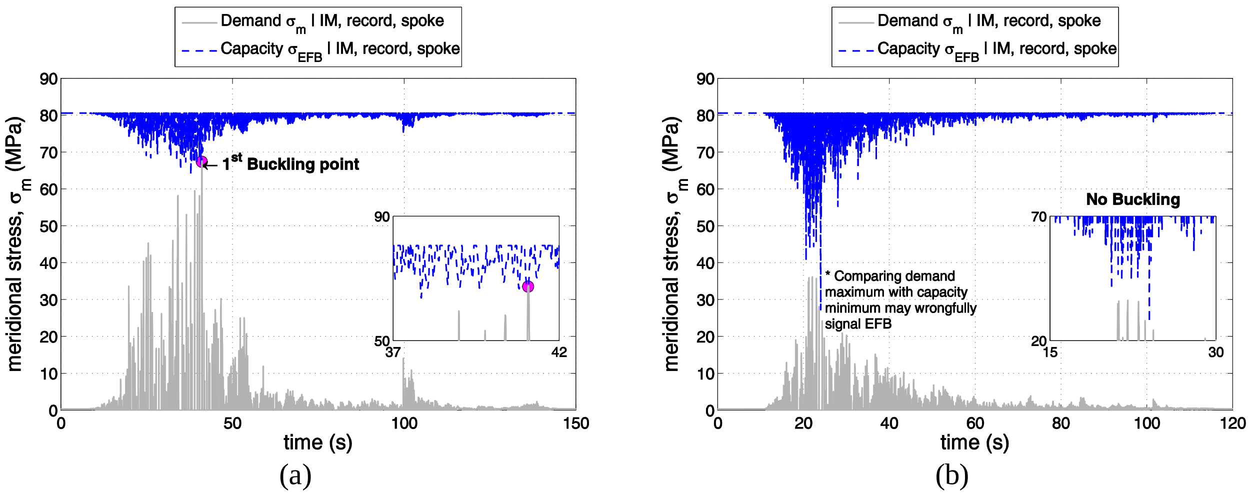

Figure 3: IM, record and spoke-specific EFB capacity versus demand response histories for the unanchored tank A (Table 1): (a) intersection among time-dependent demand and capacity signals EFB; (b) EFB capacity is not exceeded even though the associated time-independent maximum demand and minimum capacity indicate so.

Capturing EFB becomes more complex when capacity dispersion appears due to uncertainty. Given the time dependence of EFB capacity and demand, the EFB probability of exceedance for a given record, *IM* level and spoke becomes the union of the individual probabilities of EFB occurring at any single moment of time. To avoid a cumbersome bookkeeping and post-processing procedure where entire $\sigma_m(t)$ and $\sigma_{EFB}(t)$ response histories would need to be assessed, the simpler peak "demand-over-capacity" ratio exceeding unity is preferred (Figure 3). Evidently, the peak $\sigma_m(t)/\sigma_{EFB}(t)$ ratio provides the demand and capacity values that should be recorded for each spoke during every nonlinear response history analysis.

$$\mathrm{P}\left[\mathrm{EFB}\,|IM, record, spoke\right] \cong \mathrm{P}\left[\left(\max_t \frac{\sigma_m(t)}{\sigma_{EFB}(t)}\right) > 1 | IM, record, spoke\right] \tag{7}$$

The vertical component of the ground motion has not been considered in the analyses, yet the model framework can easily accommodate it. A preliminary investigation showed that the effect of vertical acceleration was evident on the EFB capacity only (not on any demand), and then for specific tanks and ground motion records. Overall, only tank B (Table 1) showed some sensitivity, becoming more prone to EFB damage.

4.5.2 Extent of damage

Of potential interest is also the extent of EFB damage, as according to studies based on detailed finite element models (e.g. [16,29]) it is highly unlikely that the examined buckling mode of failure is restrained to small arc lengths covered by a single beam-spoke. Figure 4(a), compares the EFB capacity for a given *IM* level and record to the corresponding demand along the circumference of the tank. It seems that although the buckling zone spreads on a significant number of beam spokes, there are several locations where the capacity has not been reached. Lengthwise, buckling spreads on two nearly identical (as well as symmetrical) subzones, a fact that is indicative of the system's tendency (in this case) to rock along a maximum response axis. Obviously, these results should be interpreted in tandem with experimental or finite element analysis results, as the weakening of the tank wall, not captured by the "Joystick" model, may indeed promote the spread of buckling beyond our simpler estimates.

4.5.3 EFB conditioned on the *IM* level

Figure 4(b) illustrates the EFB capacity and demand along the circumference of the tank, for a given earthquake intensity, using a set of 135 large-magnitude ordinary (i.e. non pulsive, non long-duration) ground motion pairs obtained from the PEER-NGA database [36]. The considerable variability revealed for the capacity as well as the demand indicates that there are certain records where capacity is not exceeded at any part of the tank, others where it is exceeded everywhere, and some that follow the partial violation pattern shown in Figure 4(a). One may also notice the effect of directionality that derives from the combination of longitudinal and transverse earthquake components in time (Figure 2), determining a different axis of maximum demand for each ground motion pair.

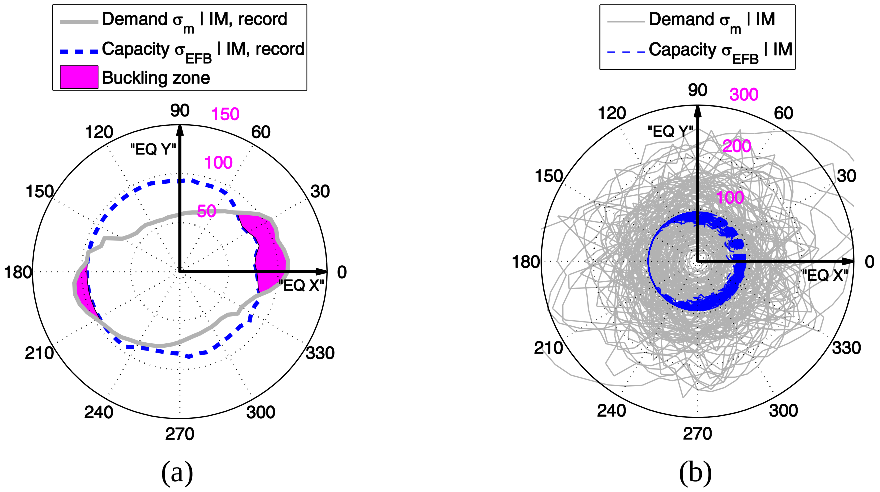

Figure 4: EFB capacity versus demand stresses (in MPa) along the circumference of the unanchored tank A (Table 1), conditioned on PGA= 0.30g: (a) single record pair and (b) 135 record pairs.

4.5.4 EFB on the IDA plane

A better understanding regarding the detailed representation of EFB may be obtained through IDA [7], for the record suite previously adopted. The results shown in Figure 5(a) display the single-record (pair) IDA curves using the meridional stress as an appropriate *EDP* and the peak ground acceleration (*PGA*) as a representative *IM*. It should be noted that the response history analysis is performed using both longitudinal and transverse ground motion accelerograms (Figure 2), which implies that a unique scale factor has been applied on both accelerograms for each ground motion pair and that the *PGA* refers to the geometric mean of the two. The light-coloured solid lines form the demand for an arbitrary edge-spring on the "Joystick" model, while the dark dashed ones depict the associated buckling capacity variability for the given range of *IM* levels. The initial buckling capacity at rest (i.e. for a *PGA*=0) refers to the static load case of the liquid storage system, where the maximum internal pressure equals the corresponding hydrostatic. For larger *PGA* estimates, the impulsive pressure adds on to the hydrostatic component on the compressive side of the tank, which results in a significant reduction of the EFB capacity. Intersection among capacity and demand curves for each record provides the individual EFB limit state capacity points.

Figure 5(b) shows a more comprehensive representation of EFB. In particular, the entire capacity-demand space is presented through the single-record IDAs for every beam-spoke that forms the base plate of the "Joystick" model. EFB capacity points that represent failure on *any* single spoke (i.e. 1st-spoke failure pattern) are compared to a more extensive state of damage that spreads on 50% of the tank circumference (i.e. multi-spoke failure pattern). The 50% spread of damage is arbitrarily chosen and thus a different value could be used upon the availability of relevant (experimental/structural analysis) data. Comparing the two approaches reveals a clear-yet marginal-shift of the multi-spoke failure to higher *PGA* estimates, which practically triggers the discussion between localised and widely spread buckling.

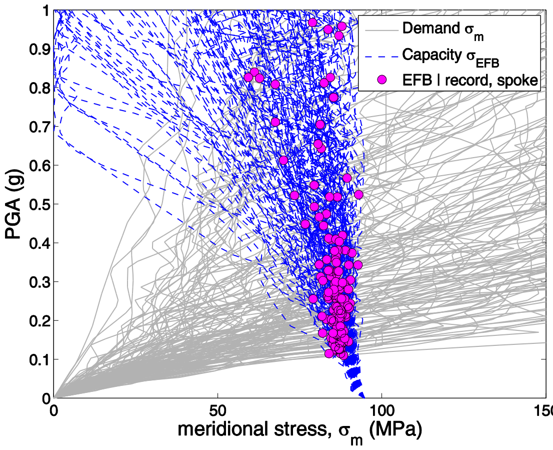

(a)

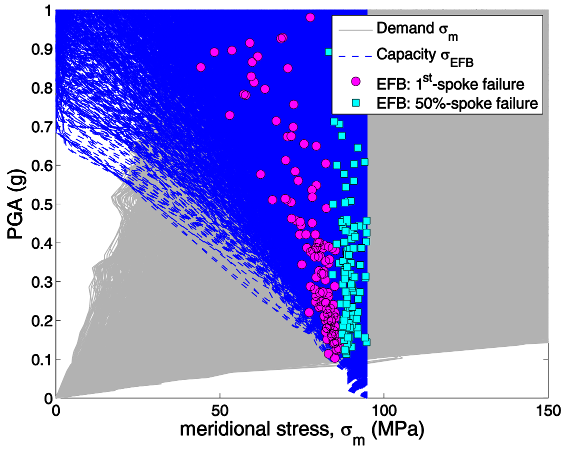

(b)

Figure 5: (a) EFB demand versus capacity single-record (pair) IDA curves for an arbitrarily chosen edge-spring on the "Joystick" model. (b) Single versus multi-spoke EFB failure on the demand-capacity space formed by single-record (pair) IDA curves for the entire set of edge-springs found on the base of the "Joystick" model. The results refer to the unanchored tank A (Table 1).

Traditionally, common approaches for capturing buckling modes conservatively rely on the first point/element on a structure whose demand exceeds the prescribed capacity (e.g. single-spoke failure). Although for the purpose of this study the single-spoke pattern is conservatively adopted to signal EFB, Figure 5(b) highlights the abilities of the "Joystick" model to capture limit state capacities that are defined based on the extent of EFB (or any other) mode of failure and could potentially provide a more refined approach in terms of loss. In reality, EFB induces a local instability on the actual tank (not captured by the "Joystick" model) that causes a modification of its properties such that buckling is potentially easier to spread than is shown herein. This is generally tough to quantify, and thus the purpose of this analysis is to indicatively shed some light on the spread of buckling, pending further calibration. The estimate provided remains a useful approximation barring the use of more complex models.

DOI: XX

Table 1: Properties of the tanks examined [29].

Properties	Variable description	Notation (units)	Numerical values		
			Tank A	Tank B	Tank C
Tank	Radius	R_t (m)	13.9	23.47	6.1
	Height	h_t (m)	16.5	19.95	11.3
	Wall thickness per course	t_w (mm)	17.7;15.7;13.7;11.7; 9.7;7.8;6.4;6.4;6.4	22.23;18.93;16.24;13.57; 10.9;8.22;8.0;8.0;8.0	9.6;8.0;6.4;4.8
	Base plate thickness	t_b (mm)	6.4	6.4	4.8
	Annular ring thickness	t_a (mm)	8.0	10.0	4.8
	Roof mass	m_r (ton)	35	46	19
Material	(expected) Yield strength	f_y (MPa)	280	280	280
	Steel Young's Modulus	E (GPa)	210	210	210
	Hardening ratio	a_h (%)	1	1	1
	Poisson's ratio	v (-)	0.3	0.3	0.3
Fluid	Height	h_f (m)	15.7	18.95	10.74
	Density	ρ_f (kg/m^3)	1000	1000	1000

5. DAMAGE STATES

In modern probabilistic seismic assessment framework [4] damage is discretised into a number of (typically consecutive) damage states that are chosen to represent consequences of increasing severity, based on the failure modes that a structure is prone to exhibit. For instance, design codes for buildings define performance levels similar to "Immediate Occupancy" and "Collapse Prevention". Uncontrollable socioeconomic consequences encountered after past earthquakes [37], however, establish such performance objectives totally unfit for the seismic risk evaluation of industrial facilities. For the case of liquid storage tanks, the most damaging failure modes are the ones that may result in loss of containment, while other modes are mainly confined to structural damage without leakage. Figure 6 presents the associated failure modes on the median IDA curve both for an anchored and an unanchored system (Table 1). Unlike Figure 5 where EFB is examined in detail and hence σ_m is employed as the *EDP*, in this instance the base uplift is shown instead. Although it does not directly relate to the entire set of failure modes outlined in previous sections, the intuition it provides in terms of global (system) deformation is similar to response parameters such as roof displacement and maximum inter-storey drift for buildings, thus allowing for a rough illustration of the damage progression on the tank.

A further classification based on the damage of individual components becomes quite informative, where the upper course of the tank (SL=sloshing), its lower course (EFB), the base plate (θ_{pl}), and the anchors (AN=anchorage failure) are separately examined. Table 2 presents the component-level median damage state capacities along with their associated dispersions and engineering demand parameters. In absence of relevant experimental data, the strength-based (for EFB), ductility-based (for θ_{pl}, AN) and displacement-based (for SL) approximations of the FEMA P-58 [12] guidelines are employed to derive the dispersion around the lognormally distributed capacities of the aforementioned failure modes. Given that the random variables presented in Table 2 refer to different parts of the tank, as well as that hardly any relevant data exists, correlation among the capacities of the examined failure modes has been assumed to be zero. Non-zero positive correlation may reasonably be adopted for the capacity of damage states referring to the same component, e.g. θ_{pl} capacity values for consecutive damage states at the same location (i.e. spoke) of a tank. For a more realistic representation, spatial correlation of DS capacity values among different spokes also becomes an issue. Yet, such considerations are beyond the scope of this study as they burden the post-processing considerably.

In this study, the aforementioned failure modes are appropriately combined to form four damage states of increasing severity, namely no damage (DS0), minor (DS1), severe without

DOI: XX

leakage (DS2) and loss of containment (DS3), as originally proposed in [38,39]. It should be noted that the loss of containment is generally the main concern post-earthquake, as it constitutes a paramount source of industrial accidents with severe socioeconomic and environmental consequences [24]. Still, structural damage itself (with or without leakage) is also of concern, since its aftermath is not confined to monetary losses only. The reason is that frequent earthquakes of moderate intensity, may trigger a list of actions that include drainage of the tank, repair and refill. This is often inferred as a major disruption of business, the financial impact of which cannot be ignored.

In that sense, for the case of unanchored (or self-anchored) liquid storage tanks, DS1 shall represent minor damage induced by a sloshing wave height of the contained fluid equal to the freeboard. DS2 shall refer to severe damage at any component of the tank without leakage, where the exceedance of either a sloshing wave height equal to 1.4 times the available freeboard or a plastic rotation of 0.2 rad at the base plate shall trigger the damage state violation. DS3, finally, shall provide information on the loss of containment through the exceedance of either the EFB capacity (σ_{EFB}) or the base plate plastic rotation of 0.4 rad. While some further partitioning of the loss of containment damage states based on the amount of leakage would be desirable, there is little data available to define appropriate *EDP* thresholds. As far as anchored systems are concerned, yielding on the anchors or their connection to the tank may also be considered for DS1, while fracture for DS2, as shown in Table 3. This classification reasonably conveys the extent of system damage, yet one should bear in mind that the different mechanisms involved in a single damage state may be associated with varying degrees of monetary loss or repair actions. For instance, sloshing waves whose amplitude exceeds the available freeboard represent relatively easy-to-repair damage at the top of the tank, compared to the exceedance of a plastic rotation limit at the base, even though both might be categorised as moderate damage. Therefore, it becomes more informative to also classify damage based on the actual component that has failed, as shown in Table 2.

Table 2: Component-level DS classification for anchored and unanchored liquid storage tanks.

Component	Failure Mode Notation	Median EDP Capacity ($EDP_{C,50\%}$)	Reference	Dispersion* [12]
Upper tank course	SL	$1.0\times d_f$ (m)	[3]	0.20
		$1.4\times d_f$ (m)	[3]	0.20
Lower tank course	EFB	σ_{EFB} (MPa)	[2]	0.31
Base plate	θ_{pl}	0.2 (rad)	[2]	0.51
		0.4 (rad)	[31]	0.51
Anchors	AN	δ_y (mm)	-	0.51
		δ_u (mm)	-	0.51

*The standard deviation of the log values

Table 3: System-level DS classification for anchored and unanchored liquid storage tanks.

System Support Conditions	Damage States	Damage State Capacities
Anchored	DS1	$1.0\times d_f$ or δ_y
	DS2	$1.4\times d_f$ or θ_{pl}=0.2rad or δ_u
	DS3	σ_{EFB} or θ_{pl}=0.4rad
Unanchored	DS1	$1.0\times d_f$
	DS2	$1.4\times d_f$ or θ_{pl}=0.2rad
	DS3	σ_{EFB} or θ_{pl}=0.4rad

DOI: XX

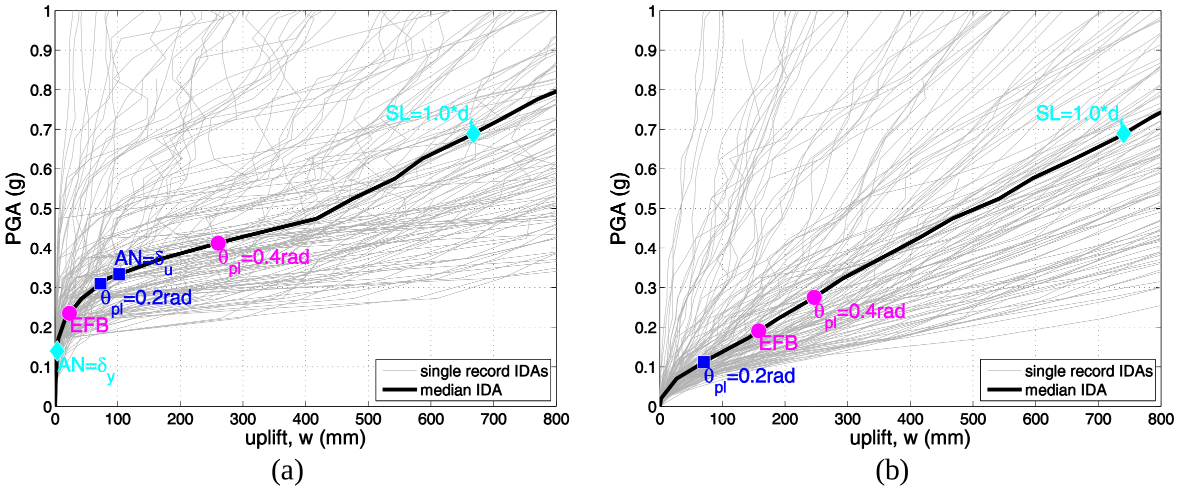

Figure 6: Single-record (pair) IDAs along with the associated failure modes on the median IDA curve for liquid storage tank A (Table 1): (a) anchored and (b) unanchored support conditions.

6. SEISMIC FRAGILITY ASSESSMENT

Under the typical assumption of lognormality for both demand (D) and capacity (C) (valid for EDP demand away from the global instability region only), the probability that the median demand exceeds the associated damage state capacity for a given level of seismic intensity, may be estimated using either of EDP or IM ordinates (i.e. EDP-basis versus IM-basis estimation [11,40]) through the standard normal cumulative distribution function Φ as:

$$\mathrm{P}[D > C \mid IM] = \Phi\left(\frac{\ln EDP(IM)_{50\%} - \ln EDP_{C,50\%}}{\beta_{EDP}}\right) = \Phi\left(\frac{\ln IM - \ln IM_{C,50\%}}{\beta_{IM}}\right) \tag{8}$$

$EDP(IM)_{50\%}$ is the median EDP demand given the IM, $EDP_{C,50\%}$ and $IM_{C,50\%}$ are the median limit state capacities expressed in EDP and IM terms respectively, while β_{EDP} and β_{IM} the total EDP and IM-basis dispersions that take into account both aleatory and epistemic sources of uncertainty (see [11] for their explicit definition).

The parameters found in Eq. (8) incorporate the IM, and as a result accurately estimating seismic fragility requires an intensity measure that characterises the structural system's response in an optimal manner. According to Luco and Cornell [41], the answer to this problem is not distinct, as the well-known criteria of sufficiency, efficiency and practicality must be satisfied. In particular, the optimal IM should render the structural response independent of seismological characteristics appearing as variables in the probabilistic seismic hazard assessment (e.g. magnitude, distance, epsilon), it should be able to reduce dispersion in the $EDP|IM$ (or $IM|EDP$) relationship and thus the number of ground motion records required to achieve the same level of accuracy, while at the same time it should be possible to compute the corresponding hazard curve. For the case of liquid storage tanks, either of the PGA and the spectral acceleration at the impulsive period ($S_a(T_i)$) is a reasonable choice due to the relatively short impulsive period (T_i); still, the convective response can only be adequately captured through the corresponding convective spectral acceleration that is poorly described by the short T_i. This is an interesting problem that requires delicate handling and is expected to be covered in a future direction of our research.

DOI: XX

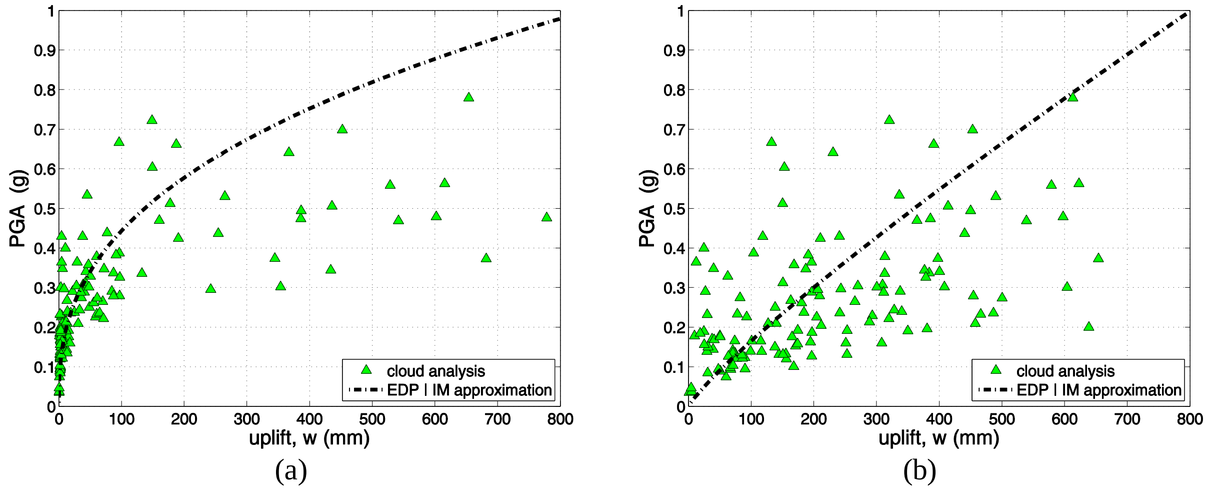

Figure 7: Cloud analysis and fitted (global) *EDP-IM* relationship for liquid storage tank A (Table 1): (a) anchored and (b) unanchored support conditions.

7. PARAMETRIC INVESTIGATION

7.1. Component-level evaluation

In order to assess the seismic fragility involved in liquid storage systems, three tanks of varying aspect ratios (h_f/R_t) are considered (Table 1), covering a range of broad to slender structural system configurations. The estimation is initially performed on a component-basis (Table 2), using the various analysis methodologies discussed above. In this instance, the liquid storage systems are considered unanchored, with the results of this process summarised in Figure 8, in terms of median *IM* capacity and the associated dispersion (see also the component fragility curves in Figure 9). Offering a detailed view of demand at each *IM* level, IDA is adopted herein as a benchmark solution to discuss the validity and applicability of a simplified (computationally inexpensive) cloud approach that utilises only a single suite of unscaled ground motions and a global power-law fit in the *EDP-IM* space (e.g. Figure 7).

Comparing the cloud analysis results to IDA presents a reasonable agreement for certain failure modes. As far as EFB is concerned, a good agreement is observed for all unanchored tanks, despite the slight reduction of the tank B cloud-based dispersion. Regarding θ_{pl} limit states (i.e. 0.2 and 0.4rad), the agreement is very good in terms of median *IM* capacity; however, the dispersions stemming from cloud analysis seem to deviate by scale factors that are in the order of 1.3-2, mostly attributed to the estimation of a single dispersion value by the global fit. Note that the maximum probability of exceedance on the IDA-based fragility output regarding the 0.4rad limit state capacity on tank C, hardly yields 20% (even for large *PGA* estimates), which implies that such a capacity is practically never reached on this particular structural system, and thus the corresponding fragility curve for cloud analysis need not be considered. Fragility parameters cannot be estimated for sloshing modes of failure, for all structural systems considered, thus proving the global fit adopted in that instance (combined with the sloshing-insufficient *IM* choice of *PGA*) to be inappropriate.

At this point one may rush into the conclusion that simplified cloud analysis cannot always be trusted within a seismic risk assessment framework, as the assumption that "certain failure modes might not be adequately captured" cannot be overruled. The truth is that some care should be exercised when employing simplified approaches within a PBEE framework. For example, the cloud method adopted is sensitive to pre-processing tasks such as the record selection and the associated scaling. These parameters essentially determine the extent of the *EDP-IM* space, and thus the ability to capture certain damage state capacities that are found in rather large response parameter values. Undeniably, our case study also suffers from such issues, as the (unscaled) record-set that has been used does not provide an adequate number of analysis data points around certain *EDP* capacities of interest, that would otherwise lead to a more accurate regression analysis output. Note that the simplified cloud-based assessment cloud also be refined by adopting a local fit in place of the global one shown in Figure 7. Despite the aforementioned problems and their rather complex nature, cloud analysis still remains probably the best alternative to IDA, for cases that the latter is deemed computationally prohibitive.

7.2. System-level evaluation

Following the comparison of the various analysis methodologies and their effect on the seismic fragility parameters, the system-level evaluation is performed for the entire set of liquid storage tanks, considering both anchored and unanchored support conditions (Table 3). The aim is to assign a single damage state that could be useful in several instances such as regional loss assessment or the assessment of an entire tank-farm, similar to the HAZUS methodology [13]. For the shake of brevity, only the IDA-based fragilities for unanchored support conditions are illustrated in Figure 9. The entire seismic fragility assessment procedure is summarised in Table 4, where parameters such as the median *IM* capacity ($IM_{C,50\%}$) and the associated (total) dispersion (β) are provided for the corresponding fragility curve construction. The dominant failure mode (DFM) as well as the order that each damage state appears during a strong ground motion, are also provided in order to highlight the complexities involved in the assessment of cylindrical liquid storage systems. Special attention is paid to the compound system-level damage states (i.e. damage states that depend on the union of the exceedance of two or more failure mode capacities, e.g. DS2 and DS3 for unanchored tanks), where a simple Monte Carlo integration is required to estimate the associated probability of exceedance [11]. A good example to appreciate the importance of this procedure can be given through the final fragility product of DS2 and DS3 for the unanchored tank A (Figure 9(b)). According to Figure 9(a), it appears that although the plastic rotation clearly dominates the response of DS2, a similar conclusion cannot be drawn for DS3 as the plastic rotation appears to influence lower *IM* levels contrary to EFB that is more probable for higher ones.

A closer look on the results of Table 4 suggests that even though the sloshing mode governs the response for all unanchored systems with respect to DS1, the corresponding response for anchored tanks is dominated by yielding of the anchor bolts, for considerably smaller median PGA estimates. DS2 on the other hand, reveals the plastic rotation as the dominant failure mode for every case of unanchored tanks, while for the case of anchored ones the prevalent response cannot be distinguished among the failure modes considered, and therefore it is deemed "inconclusive". In addition, EFB is the mode of failure that controls DS3 for all systems examined (both anchored and unanchored). The beneficial effect of the anchors is also highlighted through the seismic fragility estimation of DS2 and DS3, where each failure mode (unrelated to anchors) is developed for significantly higher intensities, as shown in Table 4. Finally, another major conclusion that can be drawn from the assessment procedure, is that the damage states developed do not follow a priori the intuitive order which dictates that increasing intensities result in increasing levels of damage. This issue of non-sequential damage states highlights the fact that certain tanks may progress directly to catastrophic levels of damage

DOI: XX

without any warning (e.g. progression through lesser damage states).

Table 4: System-level seismic fragility assessment of the tanks examined.

Tank	**DS1**			**DS2**			**DS3**			**Order of DS*i***
	$IM_{C,50\%}$ (g)	β	DFM*	$IM_{C,50\%}$ (g)	β	DFM*	$IM_{C,50\%}$ (g)	β	DFM*	
Unanchored A	0.689	1.349	SL	0.117	0.758	θ_{pl}	0.168	0.620	EFB	2-3-1
Anchored A	0.130	0.479	AN	0.274	0.383	inconclusive	0.233	0.359	EFB	1-3-2
Unanchored B	1.069	1.382	SL	0.090	0.829	θ_{pl}	0.056	0.767	EFB	3-2-1
Anchored B	0.089	0.480	AN	0.187	0.441	inconclusive	0.076	0.385	EFB	3-1-2
Unanchored C	0.468	1.012	SL	0.201	0.631	θ_{pl}	0.378	0.628	EFB	2-3-1
Anchored C	0.265	0.566	inconclusive	0.512	0.622	inconclusive	0.672	0.344	EFB	1-2-3

*Dominant Failure Mode

8. SEISMIC RISK ASSESSMENT

The ultimate goal of seismic assessment lies in the mean annual frequency (λ) estimation for any set of consequences (or decision variables in the terminology of the Cornell-Krawinkler PBEE framework [4]). This may be achieved, e.g., for monetary losses either by defining them at the global system-level in a manner similar to HAZUS [13], or by employing the more detailed local component-level DS classification and appropriate cost functions, thus adopting a format akin to FEMA P-58 [12]. With such data available, the implementation according to any of the two standards should be straightforward (see also [42]).

The simpler estimation of the MAF of discrete limit-states is normally performed through an integration on the product of the site-specific hazard function $\lambda(IM)$, typically obtained through probabilistic seismic hazard analysis (PSHA), with any of the aforementioned fragility curves (i.e. P[D>C|IM]) [40,43]:

$$\lambda(DS) = \int_{IM} \mathrm{P}[D > C|IM]\,|\mathrm{d}\lambda(IM)| \tag{9}$$

For the purposes of this study, the Elefsina, Greece hazard curve is adopted [44], targeting a site of major refineries. The results shown in Figure 10 summarise the component as well as system-level seismic risk assessment in terms of mean return period (T_r=1/λ). As expected, from a qualitative perspective, the results are not any different from the ones shown in the seismic fragility section (Figure 9). In fact, the discrepancies noticed among the various structural systems and analysis methodologies are nearly identical. However, the view they offer is of a slightly different nature, as they essentially provide an indication of how rare a certain failure mode (or state of damage) is on the site under investigation, or in other words the failure modes that each system is prone to experience during earthquakes consistent with the site. What really matters in this case is the order of magnitude of the various return periods.

For instance, sloshing modes of failure can generally be considered rare events (for the given combination of site and tanks), as the mean return periods they develop are considerably higher compared to plastic rotation and EFB. The well-known return periods that correspond to "10% in 10 years" and "10% in 50 years" probability of exceedance (i.e. 95 and 475 years respectively) are also provided as reference lines, potentially useful as DS1 and DS2 performance targets respectively. As a general remark, the system-level results closely follow the worst of the relevant component-level ones, unless the dominant failure mode is highly inconclusive. At the same time, the majority of failure modes develop return periods that cannot even capture the indicative "10% in 10 years" objective, which highlights the vulnerability of the structural systems considered against the chosen site hazard. Catastrophic damage (i.e. DS2,

DOI: XX

DS3) can be several times more probable than light sloshing damage (i.e. DS1 for unanchored tanks), a direct consequence of the long convective period component that is not sufficiently excited by the moderate magnitude events and the rocky profile of the Elefsina site. The aforementioned observation stands regardless of the analysis approach, despite the considerable differences in terms of mean return period.

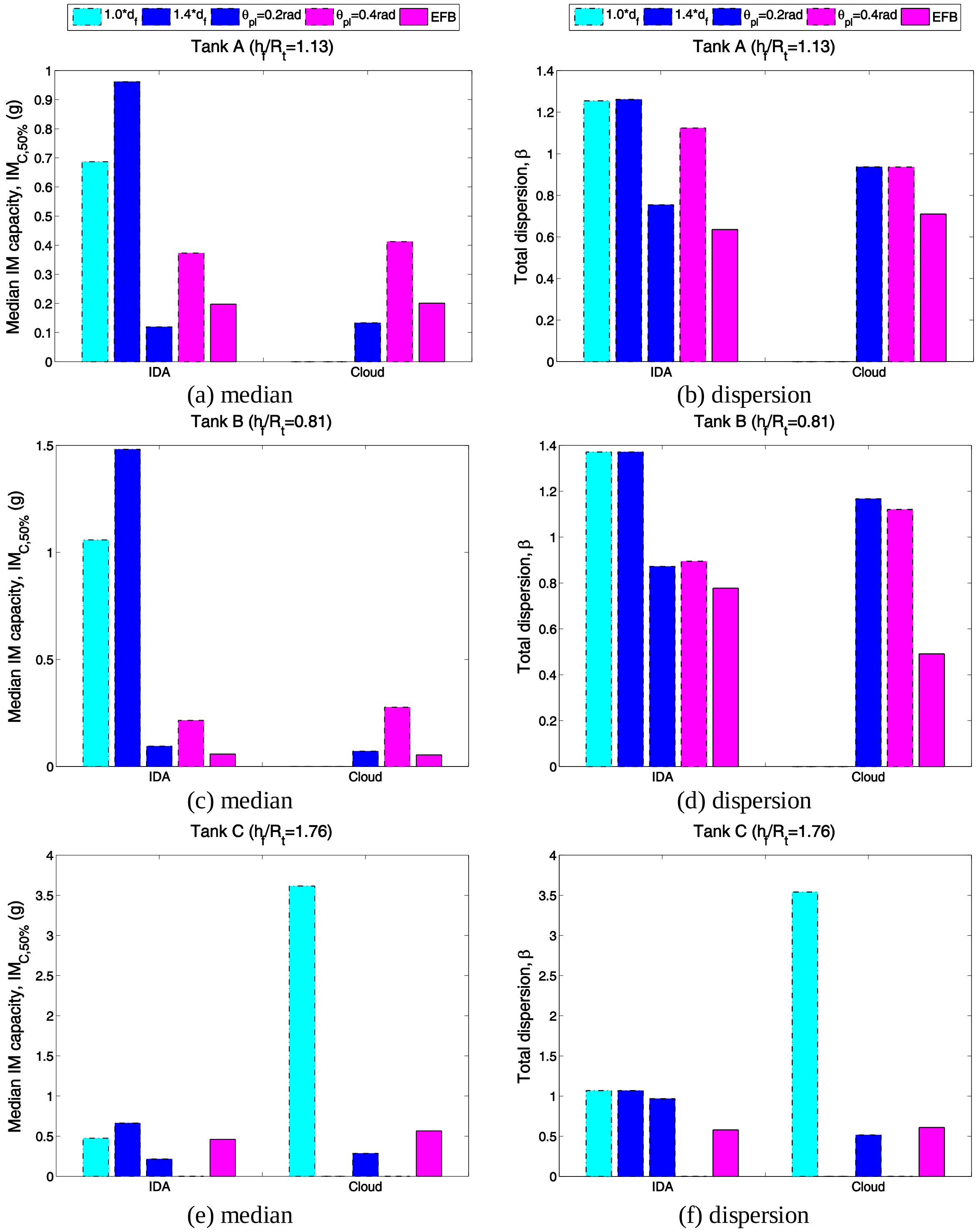

Figure 8: IDA versus cloud-based component-level seismic fragility evaluation: [(a), (c), (e)] median *IM* capacity and [(b), (d), (f)] total dispersion. The results refer to the liquid storage tanks of Table 1 for unanchored support conditions.

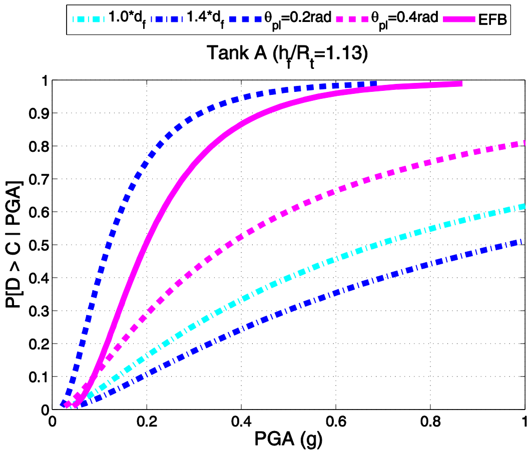

(a) component

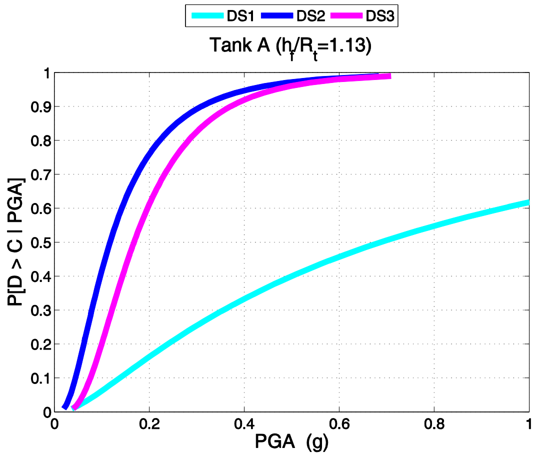

(b) system

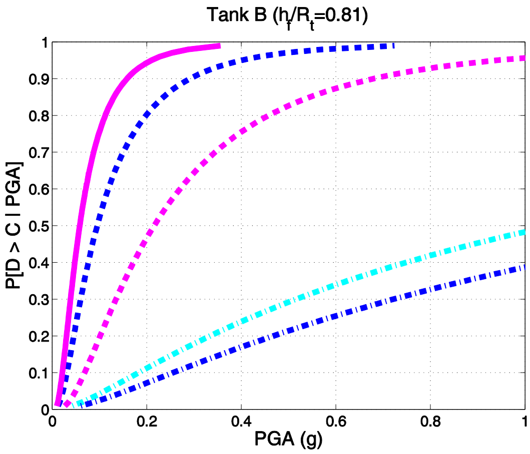

(c) component

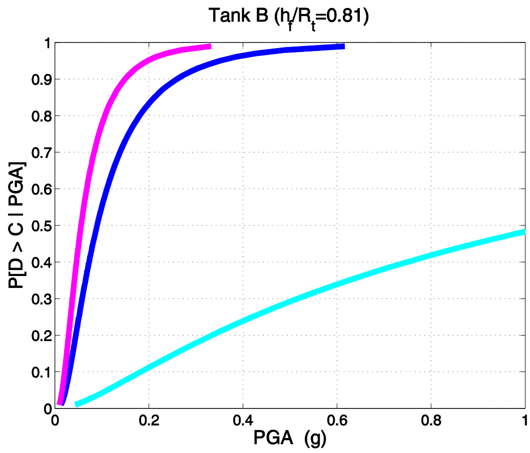

(d) system

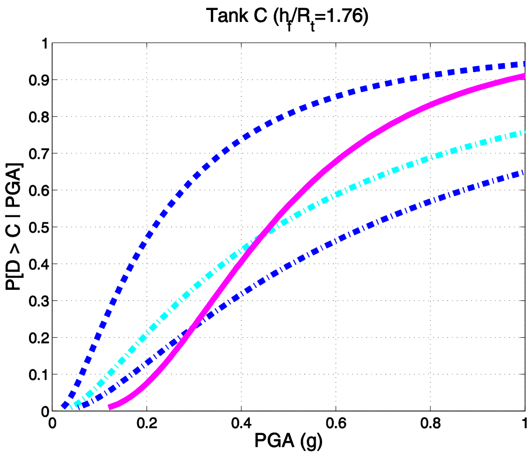

(e) component

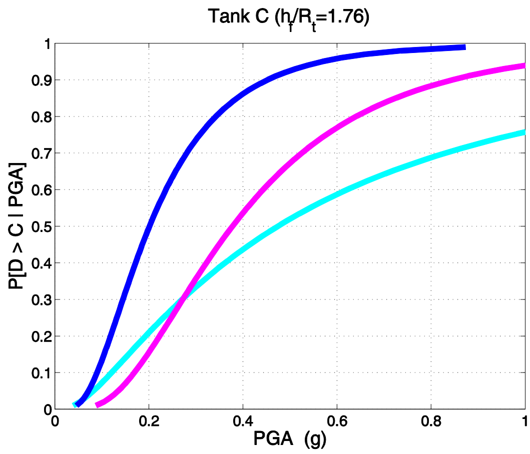

(f) system

Figure 9: IDA-based component [(a), (c), (e)] versus system-level [(b), (d), (f)] seismic fragility evaluation. The results refer to the liquid storage tanks of Table 1 for unanchored support conditions.

DOI: XX

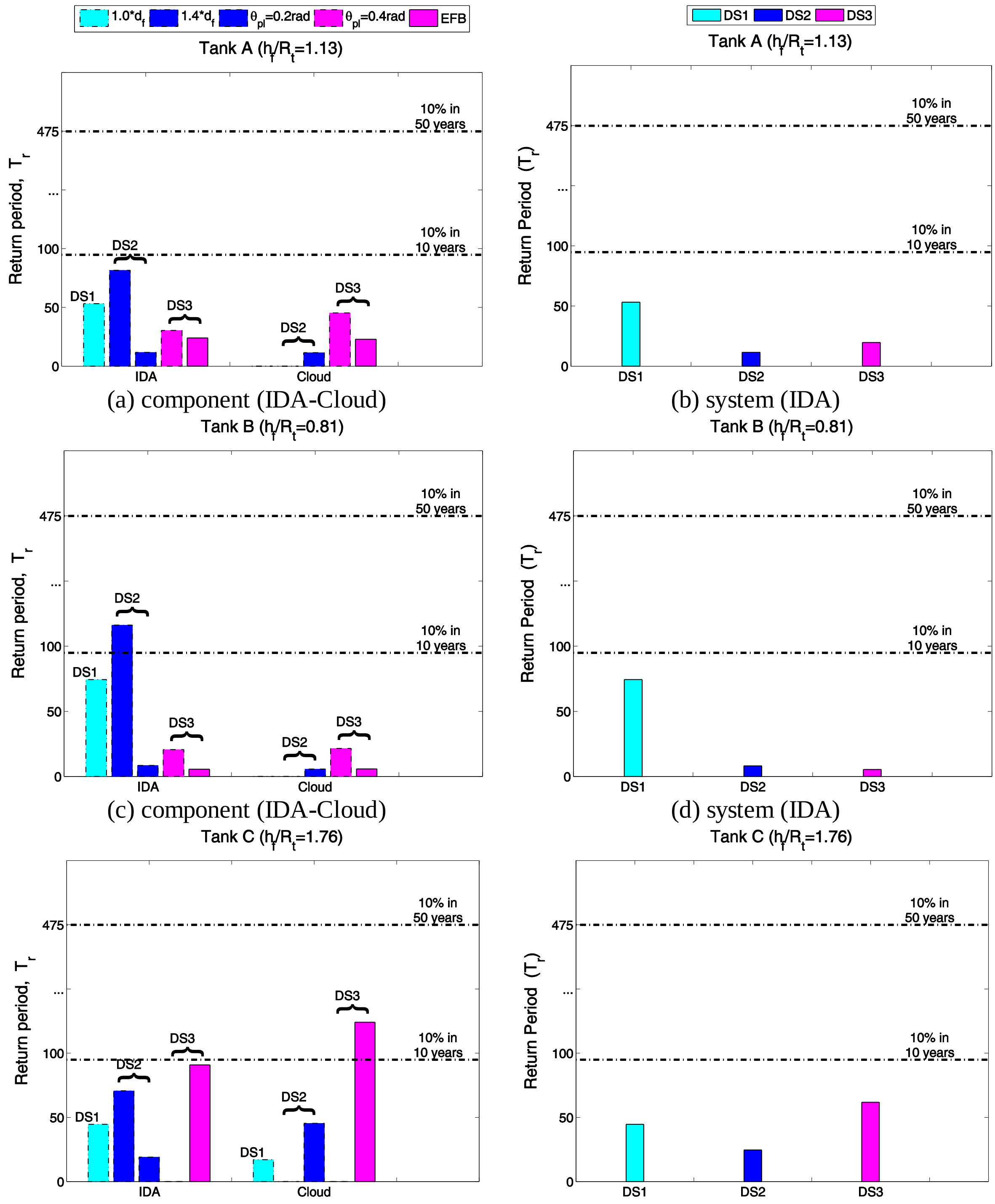

(a) component (IDA-Cloud)

(b) system (IDA)

(c) component (IDA-Cloud)

(d) system (IDA)

(e) component (IDA-Cloud)

(f) system (IDA)

Figure 10: [(a), (c), (e)] Component (IDA and cloud) versus [(b)-(d)-(f)] system-level (IDA) mean return period evaluation. The results refer to the liquid storage tanks of Table 1 for unanchored support conditions.

9. CONCLUSIONS

A reliability PBEE assessment methodology has been developed using a simplified surrogate model for liquid storage tanks. Both component and system-level damage states are outlined,

DOI: XX

favouring the seismic risk assessment of a single liquid storage unit or an entire group of tanks, respectively. Using the simplified cloud analysis to determine the *EDP-IM* relationship, and thus the corresponding fragility curves and mean return period, presents a fairly straightforward and rapid assessment approach, on the onset that some margin of error cannot be avoided compared to more refined dynamic analysis methods such as IDA. In most cases, the margin of error can further be improved by considering a larger number of records or even through rigorous post-processing techniques (e.g. a more refined local fit). The benchmark solution adopted herein through IDA provides a detailed representation of the *EDP-IM* space, although it is slightly more expensive from a computational point of view (under the condition that a surrogate model is available). On the downside, post-processing the IDA output is considerably more demanding, especially if *IM* stipes are not available [7]. Regardless of the analysis approach, EFB requires special attention, not only regarding the demand but also the capacity representation. Their underlying (negative) correlation makes the buckling capacity point substantially more difficult to determine, while at the same time suggests that this problem can probably be effectively tackled using a 3D surrogate model. Finally, unlike well-studied structural systems (e.g. moment resisting frames) where increasing seismic intensity triggers higher states of damage, the progression of failure on liquid storage tanks is non-sequential (using the limit state capacities considered), as quite often a higher damage state appears first, hinting at the onset of severe damage with little or no warning.

ACKNOWLEDGEMENTS

This research has been co-financed by the European Union (European Social Fund – ESF) and Greek national funds through the Operational Program "Education and Lifelong Learning" of the National Strategic Reference Framework (NSRF) - Research Funding Program: **THALES**. Investing in knowledge society through the European Social Fund.

REFERENCES

1. Krausmann E, Cruz AM. Impact of the 11 March 2011, Great East Japan earthquake and tsunami on the chemical industry. *Natural Hazards* 2013; **67**(2): 811–828. DOI: 10.1007/s11069-013-0607-0.
2. CEN. *Eurocode 8: Design of structures for earthquake resistance–Part 4: Silos, tanks and pipelines*. vol. 3. Brussels: 2006.
3. American Petroleum Institute. *Seismic Design of Storage Tanks - Appendix E, Welded Steel Tanks for Oil Storage*. vol. 552. API 650, 11th Edition, Washington, D.C.: 2007.
4. Cornell CA, Krawinkler H. Progress and Challenges in Seismic Performance Assessment. *PEER Center News* 2000; **3**(2): 1–4.
5. Yang TY, Moehle J, Stojadinovic B, Der Kiureghian A. Seismic Performance Evaluation of Facilities: Methodology and Implementation. *Journal of Structural Engineering* 2009; **135**(10): 1146–1154. DOI: 10.1061/(ASCE)0733-9445(2009)135:10(1146).
6. Cornell CA. Engineering Seismic Risk Analysis. *Bulletin of the Seismological Society of America* 1968; **58**(5): 1583–1606.
7. Vamvatsikos D, Cornell CA. Incremental dynamic analysis. *Earthquake Engineering & Structural Dynamics* 2002; **31**(3): 491–514. DOI: 10.1002/eqe.141.
8. Luco N, Bazzurro P. Does amplitude scaling of ground motion records result in biased nonlinear structural drift responses? *Earthquake Engineering & Structural Dynamics* 2007; **36**(13): 1813–1835. DOI: 10.1002/eqe.695.
9. Jalayer F. Direct Probabilistic Seismic Anaysis: Implementing Non-linear Dynamic Assessments.

Ph.D. dissertation, Dept. of Civil and Environmental Engineering, Stanford Univ., Stanford, CA, 2003.

10. Baker JW, Cornell CA. Spectral shape, epsilon and record selection. *Earthquake Engineering and Structural Dynamics* 2006; **35**(9): 1077–1095. DOI: 10.1002/eqe.571.
11. Bakalis K, Vamvatsikos D. Seismic Fragility Functions via Nonlinear Dynamic Methods. *Earthquake Engineering & Structural Dynamics* 2016; (Submitted).
12. FEMA. *Seismic Performance Assessment of Buildings*. vol. 1. FEMA P-58, Prepared by the Applied Technology Council for the Federal Emergency Management Agency, Washington D.C: 2012.
13. FEMA. *HAZUS-MH MR4 Multi-hazard Loss Estimation Methodology, Technical Manual*. Washington D.C.: 2003.
14. American Lifelines Alliance. *Seismic fragility formulation for water systems: Part 1-Guideline*. ASCE: 2001.
15. American Lifelines Alliance. *Seismic Fragility Formulation for Water Systems Part 2-Appendices*. ASCE: 2001.
16. Buratti N, Tavano M. Dynamic buckling and seismic fragility of anchored steel tanks by the added mass method. *Earthquake Engineering & Structural Dynamics* 2014; **43**(1): 1–21. DOI: 10.1002/eqe.2326.
17. Talaslidis DG, Manolis GD, Paraskevopoulos E, Panagiotopoulos C, Pelekasis N, Tsamopoulos JA. Risk analysis of industrial structures under extreme transient loads. *Soil Dynamics and Earthquake Engineering* 2004; **24**(6): 435–448. DOI: 10.1016/j.soildyn.2004.02.003.
18. O'Rourke MJ, So P. Seismic Fragility Curves for On-Grade Steel Tanks. *Earthquake Spectra* 2000; **16**(4): 801–815. DOI: 10.1193/1.1586140.
19. Salzano E, Iervolino I, Fabbrocino G. Seismic risk of atmospheric storage tanks in the framework of quantitative risk analysis. *Journal of Loss Prevention in the Process Industries* 2003; **16**(5): 403–409. DOI: 10.1016/S0950-4230(03)00052-4.
20. Berahman F, Behnamfar F. Seismic Fragility Curves for Un-Anchored On-Grade Steel Storage Tanks: Bayesian Approach. *Journal of Earthquake Engineering* 2007; **11**(2): 166–192. DOI: 10.1080/13632460601125722.
21. Iervolino I, Fabbrocino G, Manfredi G. Fragility Of Standard Industrial Structures By a Response Surface Based Method. *Journal of Earthquake Engineering* 2004; **8**(6): 927–945. DOI: 10.1080/13632460409350515.
22. Salzano E, Garcia Agreda A, Di Carluccio A, Fabbrocino G. Risk assessment and early warning systems for industrial facilities in seismic zones. *Reliability Engineering & System Safety* 2009; **94**(10): 1577–1584. DOI: 10.1016/j.ress.2009.02.023.
23. Razzaghi MS, Eshghi S. Probabilistic Seismic Safety Evaluation of Precode Cylindrical Oil Tanks. *Journal of Performance of Constructed Facilities* 2015; **29**(6): 4014170. DOI: 10.1061/(ASCE)CF.1943-5509.0000669.
24. Fabbrocino G, Iervolino I, Orlando F, Salzano E. Quantitative risk analysis of oil storage facilities in seismic areas. *Journal of Hazardous Materials* 2005; **123**(1–3): 61–69. DOI: 10.1016/j.jhazmat.2005.04.015.
25. CEN. *Eurocode 8 : Design of structures for earthquake resistance - Part 1: General rules, seismic actions and rules for buildings (EN 1998-1:2004)*. vol. 1. CEN, Brussels: 2004.
26. Haroun MA. Vibration studies and tests of liquid storage tanks. *Earthquake Engineering & Structural Dynamics* 1983; **11**(2): 179–206. DOI: 10.1002/eqe.4290110204.
27. Malhotra PK. Practical Nonlinear Seismic Analysis of Tanks. *Earthquake Spectra* 2000; **16**(2): 473–492. DOI: 10.1193/1.1586122.
28. Cortes G, Prinz GS. Seismic fragility analysis of large unanchored steel tanks considering local instability and fatigue damage. *Bulletin of Earthquake Engineering* 2017; **15**(3): 1279–1295. DOI: 10.1007/s10518-016-9984-6.
29. Bakalis K, Fragiadakis M, Vamvatsikos D. Surrogate Modeling for the Seismic Performance Assessment of Liquid Storage Tanks. *Journal of Structural Engineering* 2017; **143**(4): 4016199. DOI: 10.1061/(ASCE)ST.1943-541X.0001667.
30. Malhotra PK, Veletsos AS. Beam Model for Base-Uplifting Analysis of Cylindrical Tanks. *Journal*

of Structural Engineering 1994; **120**(12): 3471–3488. DOI: 10.1061/(ASCE)0733-9445(1994)120:12(3471).

31. Cortés G, Nussbaumer A, Berger C, Lattion E. Experimental determination of the rotational capacity of wall-to-base connections in storage tanks. *Journal of Constructional Steel Research* 2011; **67**(7): 1174–1184. DOI: 10.1016/j.jcsr.2011.02.010.
32. Habenberger J. Fluid damping of cylindrical liquid storage tanks. *SpringerPlus* 2015; **4**(1): 515. DOI: 10.1186/s40064-015-1302-2.
33. Rotter JM. Elephant's foot buckling in pressurised cylindrical shells. *Stahlbau* 2006; **75**(9): 742–747. DOI: 10.1002/stab.200610079.
34. Malhotra PK, Veletsos AS. Uplifting Response of Unanchored Liquid-Storage Tanks. *Journal of Structural Engineering* 1994; **120**(12): 3525–3547. DOI: 10.1061/(ASCE)0733-9445(1994)120:12(3525).
35. Malhotra PK, Veletsos AS. Uplifting Analysis of Base Plates in Cylindrical Tanks. *Journal of Structural Engineering* 1994; **120**(12): 3489–3505. DOI: 10.1061/(ASCE)0733-9445(1994)120:12(3489).
36. Ancheta T, Darragh R, Stewart J, Seyhan E, Silva W, Chiou B, *et al. PEER NGA-West2 Database, Technical Report PEER 2013/03*. Pacific Earthquake Engineering Research Center, Berkeley, CA: 2013.
37. Girgin S. The natech events during the 17 August 1999 Kocaeli earthquake: aftermath and lessons learned. *Natural Hazards and Earth System Science* 2011; **11**(4): 1129–1140. DOI: 10.5194/nhess-11-1129-2011.
38. Vathi M, Karamanos SA, Kapogiannis I, Spiliopoulos K. Performance Criteria for Liquid Storage Tanks and Piping Systems Subjected to Seismic Loading. *Proceedings of the ASME 2015 Pressure Vessels & Piping Division Conference*, Boston, Massachusetts, USA: 2015.
39. Risk Assessment for the Seismic protection Of industRial facilities, THALES 2015; . http://excellence.minedu.gov.gr/thales/en/thalesprojects/379422.
40. Vamvatsikos D, Cornell CA. Applied Incremental Dynamic Analysis. *Earthquake Spectra* 2004; **20**(2): 523–553. DOI: 10.1193/1.1737737.
41. Luco N, Cornell CA. Structure-Specific Scalar Intensity Measures for Near-Source and Ordinary Earthquake Ground Motions. *Earthquake Spectra* 2007; **23**(2): 357–392. DOI: 10.1193/1.2723158.
42. D'Ayala D, Meslem A, Vamvatsikos D, Porter K, Rossetto T. *Guidelines for Analytical Vulnerability Assessment - Low/Mid-Rise Buildings*. Vulnerability Global Component Project: 2015. DOI: 10.13117/GEM.VULN-MOD.TR2014.12.
43. Vamvatsikos D. Derivation of new SAC/FEMA performance evaluation solutions with second-order hazard approximation. *Earthquake Engineering & Structural Dynamics* 2013; **42**(8): 1171–1188. DOI: 10.1002/eqe.2265.
44. Giardini D, Woessner J, Danciu L, Crowley H, Cotton F, Grünthal G, *et al*. Seismic Hazard Harmonization in Europe (SHARE): Online Data Resource 2013; . DOI: 10.12686/SED-00000001-SHARE.

